Fachtagung "Experimentelle Strömungsmechanik"
7.–9. September 2021, Bremen

Filmdickenvermessung mittels Interferenz an dynamischen Drei-Phasen-Kontaktlinien

Establishing interferometry to measure film thicknesses near moving three phase contact lines

L. Bermel, J. Hussong
TU Darmstadt
Institut für Strömungslehre und Aerodynamik
Alarich-Weiß-Straße 10, 64287 Darmstadt

Interferometrie, Filmdicke, Kontaktlinie, Benetzung, Entnetzung, Kontaktwinkel
Interferometry, film thickness, three phase contact line, wetting, de-wetting, contact angle

Summary

The paper demonstrates the capabilities of colour interferometry for thin fluid film thickness and contact angle (θ) measurements. To test the technique a generic experiment of a wetting and de-wetting 3 phase contact line of isopropanol on an anodized metal surface is performed. Instantaneous thin film surface shapes are reconstructed near the 3 phase contact line. Microscopic contact line angles are deduced from the results, which agree with contact angle hysteresis known from literature for dynamic contact angles. Larger contact angles are measured for advancing contact lines and generally smaller but wider spread contact angles for the receding contact line. The method shows the capability to be applied in wetting on complex geometries such as in corners and other industrial applications.

Introduction

The shape of moving 3 phase contact lines gives insights in the ability of fluids to wet and de-wet substrates. Wetting processes are characterized by the dynamic contact angle (θ_{dyn}). Models to link θ_{dyn} to θ_{static} and the capillary number (Ca) exist for Newtonian fluids, where Ca is a function of the 3 phase contact line velocity and liquid properties (Kistler 1993). This shows the importance to reconstruct dynamic 3 phase contact lines to gather instantaneous information about θ_{dyn} and the velocity of the 3 phase contact line. The interferometric set-up of this paper shows to be capable to reconstruct the surface with spatial resolution in the sub-μm range. The self-developed algorithm to transform the interferometric images to 3D surfaces is tested and demonstrated through an advancing and receding isopropanol contact line on an anodized metal substrate. Results are obtained using an instantaneous advancing and receding surface to extract surface slices and contact angles as a function of normal velocity.

Experimental procedure

This section is separated in two parts. The first part describes the mechanical and optical set-up followed by details about the calibration method used during the experiments. The second part is complemented by information on the substrate, the fluid and the imposed flow.

GALA e.V., Karlsruhe, Germany, ISBN 978-3-9816764-7-1

Mechanical and optical set-up

The experimental set-up consists of a RGB laser and camera, an optical rail and the substrate. Figure 1 shows a schematic top view of the set-up. The continuous wave laser emits light with wavelengths 457 nm, 532 nm and 639 nm through an optical rail. The optical components are a polarizer, diverging and converging lens, a second polarizer and a beam splitter. The beam splitter reflects the laser beams by 90 degrees onto the wetted substrate. The substrate and the fluid film surface reflect the laser beams into the RGB camera. The camera has a CMOS Color sensor with 2456 x 2054 pixels of size 3.45 μm and a frame rate of 21. A 12X zoom lens with a 2X adapter from Navitar is used. A syringe pump supplies the fluid to the vertically aligned substrate.

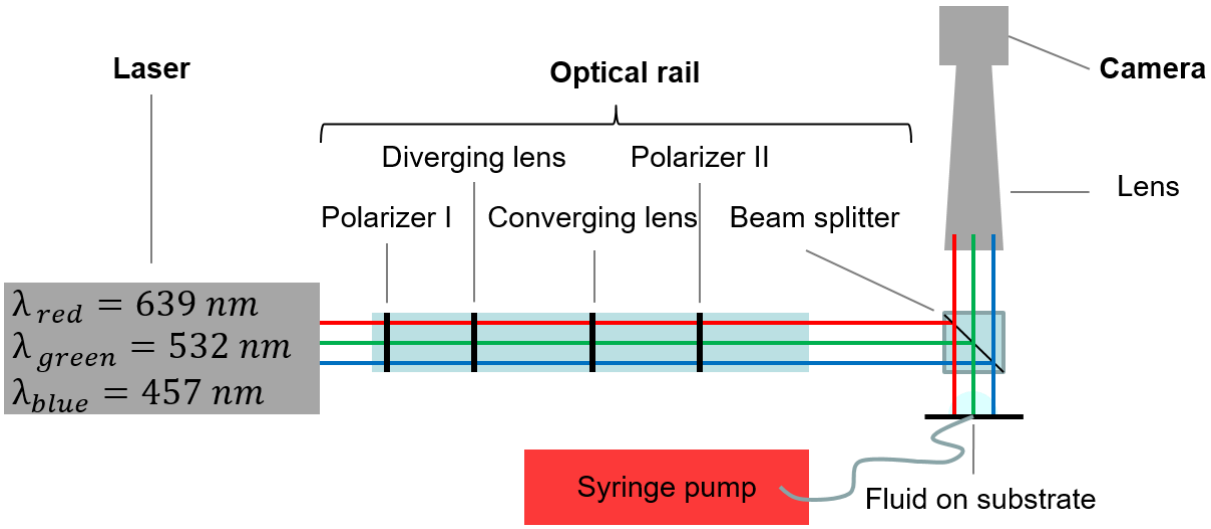

Figure 1: Experimental set-up

Choice of Field of View

The measurement system is very sensitive with regards to focal depth. Therefore, after each experiment a calibration is done. For the data used in the remainder of the paper, a pixel size of 0.6522 $\frac{\mu m}{pixel}$ is realised. Pre-tests have shown that the optical system is limited to contact angles of around 7° for a magnification of 14.

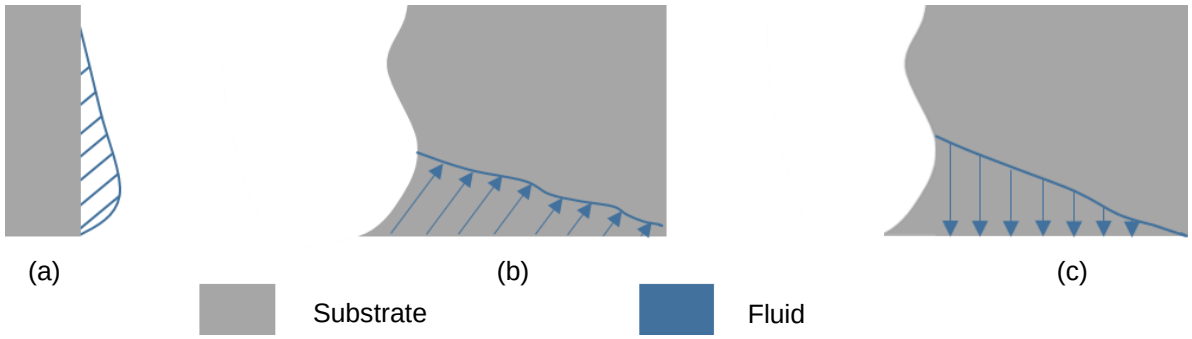

Figure 2: Measured flow regime - (a) side view of the drop-like shaped bulk fluid gathering at the bottom sharp edge of the substrate (b) front view of the wetting regime of the advancing contact line and the schematic velocities at the contact line (c) front view of the de-wetting regime of the receding contact line and the schematic contact line velocities

GALA e.V., Karlsruhe, Germany, ISBN 978-3-9816764-7-1

Isopropanol is used as the working fluid in combination with an anodized metal substrate. Isopropanol is supplied as a surface film to the substrate at a defined volume rate. The flow under investigation is a wetting and de-wetting isopropanol contact line. The substrate is wetted until a droplet-like shape of fluid is build up at the lower bottom side of the substrate (see Figure 2 (a) and (b)). Then the syringe pump stops and the receding contact line is measured as the bulk fluid evaporates (see Figure 2 (c)). Eventually, the whole deposited fluid evaporates and the substrate becomes dry again. At this state, the experiment is repeated using the same amount of deposited fluid.

Image processing

The experimental set-up is designed for three wavelengths. In the following work only the green wavelength is used to demonstrate the working principle. Figure 3 (a) gives an example of a raw laser image using a wavelength of 532 nm. The upper right corner shows a triangular like area of very low intensity, which implies that the region is not wetted by isopropanol. The fringe area denotes the wetted region. To obtain a continuous phase shift signal from fringe images the Fourier Method is applied (Takeda et al. 1982). The spatial image is transformed to the frequency domain. Hence, the Fourier spectrum is divided into a background term, a modulation term and a local phase shift term. The local phase shift term is filtered as it contains information on the film thickness. Using this result, the spatial distribution of phase shifts (φ) is obtained as given in Figure 3 (b). This phase ranges from $-\pi$ to π as the algorithm only sees the spatial intensity distribution. It is called the *wrapped phase* and is denoted by φ_{wr}.

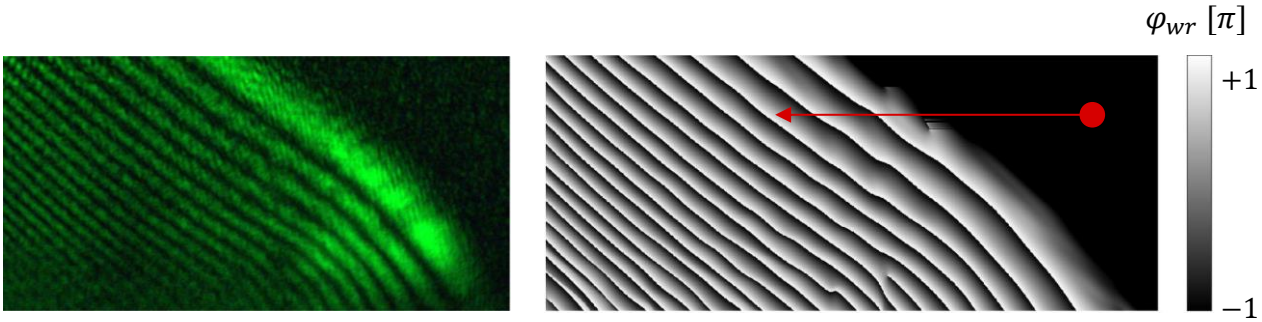

(a) (b)

Figure 3: Interference pattern - (a) raw image, (b) wrapped phase (φ_{wr}) attained by FFT

Figure 3 shows that the phase shift jumps from π to -π when the film thickness crosses a multiple of the half laser light wavelength. Hence, a phase unwrapping algorithm is applied which adds 2π to the wrapped phase as soon as a jump from π to $-\pi$ is detected. There are many unwrapping algorithms in literature, which become in general more complex with increasing curvature of the fringes. For the fringe pattern of Figure 3 (b) a line by line unwrapping algorithm is implemented. The algorithm always starts at zero thickness and then continuous along a horizontal line in direction of the surface as indicated with the red dot and arrow in Figure 3 (b). If a jump of 2π is detected within a certain tolerance level, then 2π is added to the phase for the remainder of the horizontal line. This results in the *unwrapped phase* denoted by φ_{uwr} as shown in Figure 4 (a). A relation between the thickness t_{film} and φ_{uwr} is established by Eq.1. The phase shift calculated in Figure 3 (b) contains information about the difference in optical path length of the reflected laser beams from the substrate and the fluid surface in terms of the light wavelength used. In every 2π the difference is one wavelength of the light source in use. The optical path difference consist of two times the distance between the substrate surface and the fluid film thickness. Therefore every 2π in phase shift imply a film thickness

GALA e.V., Karlsruhe, Germany, ISBN 978-3-9816764-7-1

difference of $\frac{\lambda_{green}}{2}$. This effect is accounted for in the first term of Eq. 1. The second term is a simple correction factor as the minimum phase obtained in the processing is $-\pi$. Without the correction term one would obtain negative values for t_{film} which is clearly unphysical. Applying Eq. 1 to the unwrapped phase distribution in Figure 4 (a) yields the reconstructed surface in Figure 4 (b).

$$t_{film} = \frac{\varphi_{uwr}}{2\,\pi} \cdot \frac{\lambda_{green}}{2} + \frac{\lambda_{green}}{4} \qquad \text{(Eq. 1)}$$

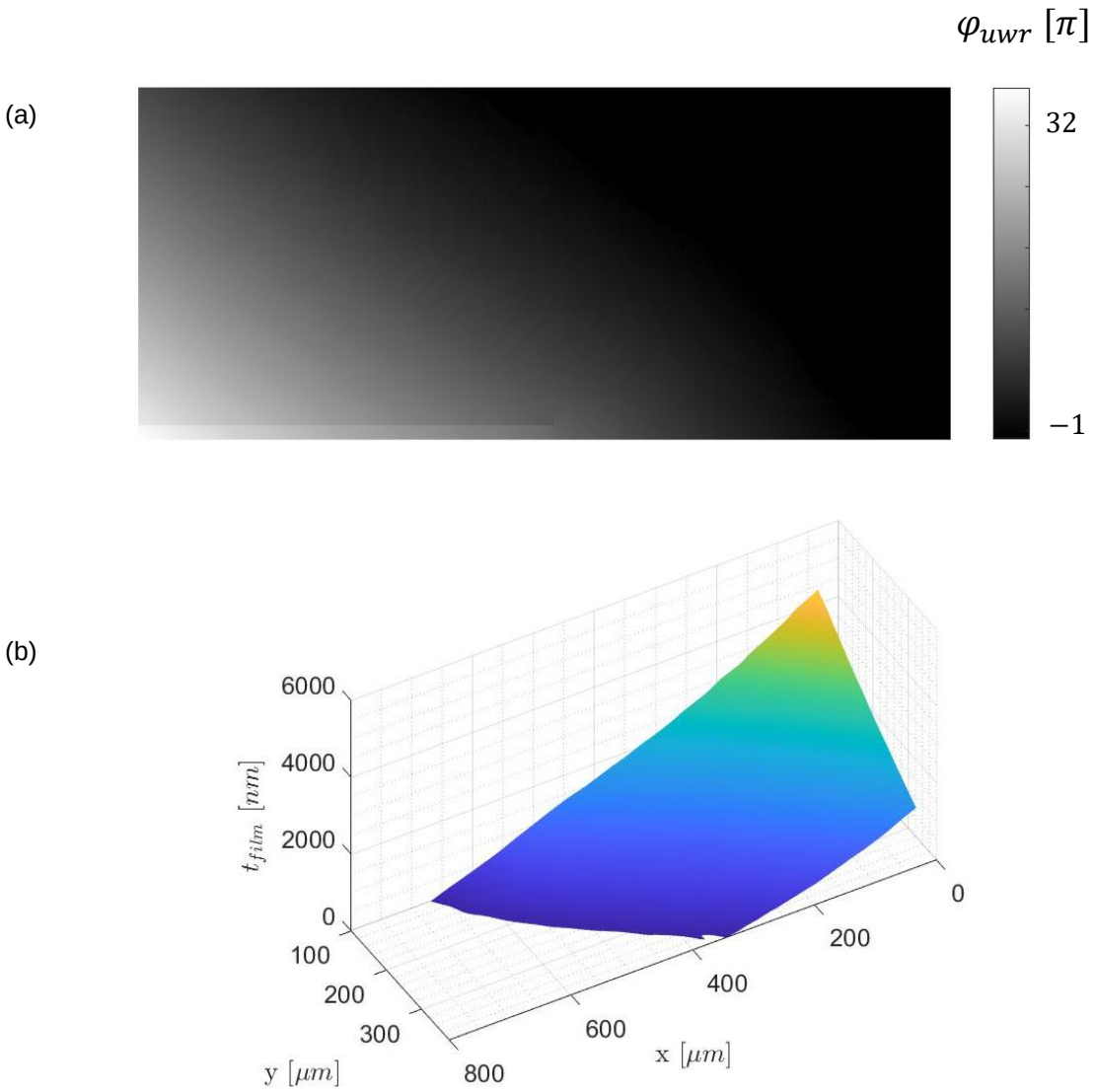

Figure 4: (a) unwrapped phase resulting from Figure 3, (b) reconstructed surface using Eq. 1

Methods and results

The acquired data are analysed by comparing the instantaneous surface shape of an advancing and receding isopropanol contact line. The thickness contours in the normal direction with respect to the contact line are analysed quantitatively and contact angles are calculated along the contour. Contact angles are calculated using a linear interpolation between the contact line

GALA e.V., Karlsruhe, Germany, ISBN 978-3-9816764-7-1

and a surface point at 130 μm distance in the normal direction with respect to the contact line. The results deal with microscopic contact angles, which is obvious from the length scales.

Contact angle and velocity distribution

This section gives an overview of the methods used to analyse the information contained in the reconstructed surfaces. As the experiment gives instantaneous surfaces it allows to determine the contact angle distribution along the contact line and the speed of the contact line at the same time. First, the 3 phase contact line is determined by the line where the reconstructed surface becomes zero as given in Figure 5 by the dashed red line. The contact line coordinates are used in the following step to determine its normal vectors to extract the contact line normal thickness lines as shown in the dotted white line on the surface in Figure 5. Contact line speed information are extracted using contact line coordinates of two time steps. The distance between two consecutive 3 phase contact line positions is calculated in the normal direction of the contact line at t_o to the corresponding point of the contact line at t_1 and using the Δt known from the camera frame rate.

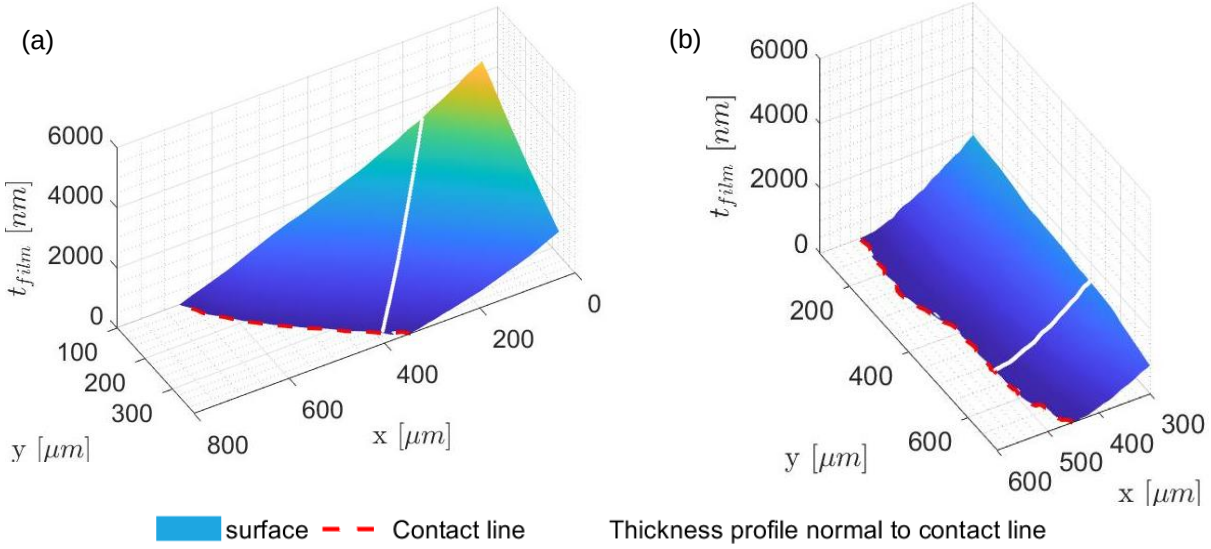

Figure 5: (a) schematic contact line and thickness distribution normal to the contact line (b) advancing contact lines at two discrete time steps

The qualitative assessment of the data is summarized in Figure 6, which shows 50 thickness profiles sampled from the instantaneous advancing and receding contact line as shown in Figure 5 (a) and (b) respectively. It is clear on first sight that the advancing profiles collapse within the whole range of normal distance with respect to the contact line. For the receding contact line the contours only collapse within the first 25 μm of normal distance with respect to the contact line. For larger film thicknesses a significant spread is seen. The average contact line velocities of the advancing and receding profiles are 345 $\frac{\mu m}{s}$ and -97 $\frac{\mu m}{s}$ respectively. This shows that the advancing contact line wets significant faster than the receding contact line dewets, which also contains data points around zero contact line speeds. An interesting aspect of the curves shown in Figure 6 are the kinks which occur approximately at every half multiple of the wavelength of 532 nm. They are more dominant in the receding profiles than in the advancing profiles. The source of this effect lies in the unwrapping algorithm and the tolerance allowed to detect the phase jumps from π to $-\pi$. Due to the discrete nature of the raw images and the noise level the pixel values in the image do not exactly reach π and $-\pi$. The effect is

GALA e.V., Karlsruhe, Germany, ISBN 978-3-9816764-7-1

more dominant in the flatter profiles as the magnitude of the tolerance is larger in relation to the unwrapped phases than in the steeper profiles.

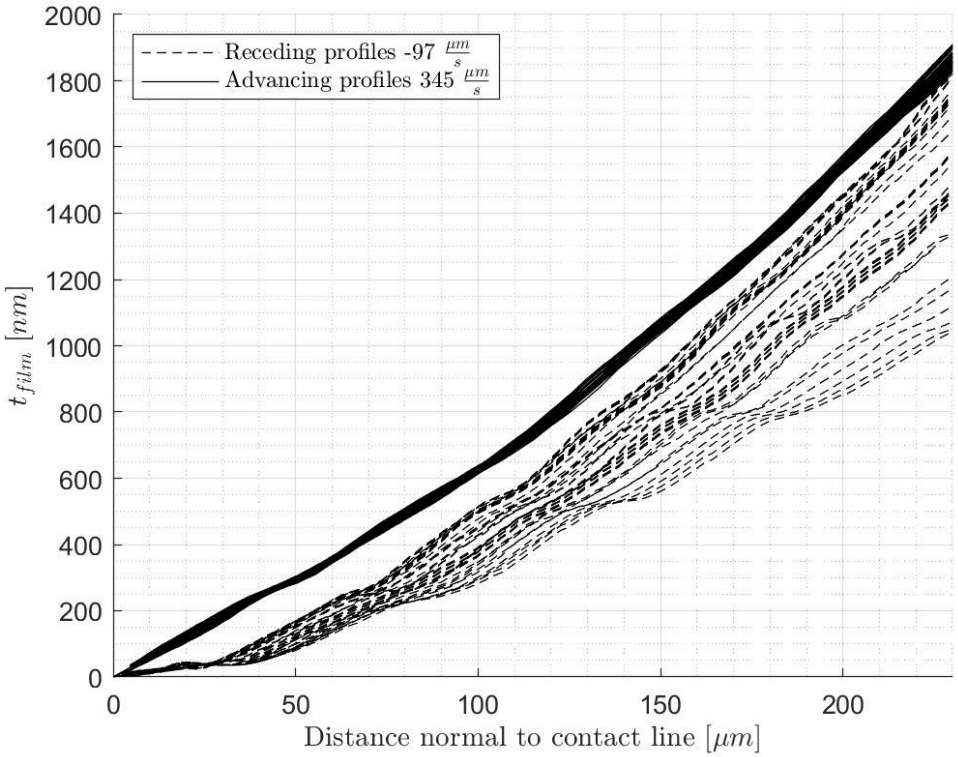

Figure 6: Thickness contours normal to the contact line extracted from the advancing and receding contact line (50 profiles each given with the average contact line speed)

This tolerance introduces measurement errors to the data. As the algorithm starts to unwrap the phase shift from zero thickness in direction of the surface, the error amplifies. This leads to the choice to quantify the error at the highest thickness value of each surface as an indication for the maximum possible error in the domain. The error is derived by the difference between the fringe count times 2 π and the value of φ_{uwr} at the coordinate of maximum thickness. The mathematical expression is given in Eq. 2.

$$err = \frac{\#_{fringes}\,(x,y)\,2\,\pi\; -\; \varphi_{uwr}(x,y)}{\#_{fringes}\,(x,y)\,2\,\pi} \qquad \text{(Eq. 2)}$$

The maximum error for the advancing contact line is calculated at the point $(x,y) = (37.8\,, 100)$ of Figure 5 (a) and is negligibly small as shown in Eq. 3. This is as expected form the very smooth profile shapes of Figure 6.

$$err_{adv}\,[\%] = \frac{17*2\pi-106.8}{17*2\pi} * 100 = 0.013 \qquad \text{(Eq. 3)}$$

The maximum error receding error is calculated at the point $(x,y) = (315.0, 99.8)$ of Figure 5 (b) and is quantified to be ~ 8% as derived in Eq. 4.

$$err_{rec}\,[\%] = \frac{7*2\pi\text{-}40.48}{7*2\pi} * 100 = 7.963 \qquad \text{(Eq. 4)}$$

GALA e.V., Karlsruhe, Germany, ISBN 978-3-9816764-7-1

This significant difference in errors suggests to implement the step detection tolerance as a function of contact angle. This will reduce the measurement error and wave-like shape distortion which become stronger for flat surfaces and lead to better results.

In the wetting community, the difference between the advancing and receding contact angle ($\theta_{hyst} = \theta_a - \theta_r$) is defined as the contact angle hysteresis, well described by Pinterich et al. 2011. In other words, this implies that repeated contact angle measurements at 3 phase contact lines moving with zero velocity result into varying values for θ. The spread of these values is proportional to the magnitude of θ_{hyst}. This typical behaviour is observed in Figure 7.

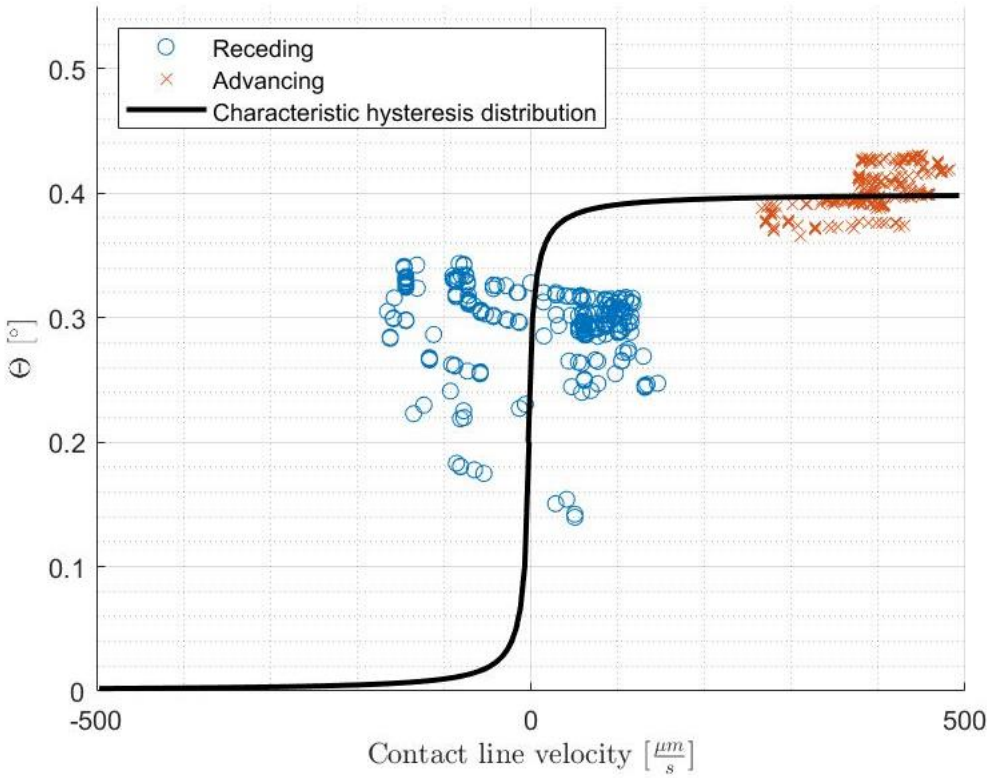

Figure 7: Contact angle vs. normal velocity measured at 130 μm distance to the contact line and schematic contact angle distribution as documented in Pascaline 2016.

It shows a scatter plot of the instantaneous contact line velocity vs. the measured contact angle. The advancing contact line shows contact angles between 0.36 and 0.43° while the receding contact line shows angle values between 0.14 and 0.35°. This clearly shows a large contact angle range around the zero velocity contact line, which doesn't show a particular pattern. This is an indication for the contact angle hysteresis phenomenon. Moreover the generally larger advancing contact angles θ_a with respect to receding contact angles θ_r agree with the findings in literature from Pinteich et al. 2011. While the concept of dynamic contact angle hysteresis is well described in literature, the authors did not find a clear convention to determine microscopic contact angles. This led to the choice to calculate the contact angle values at the distance to the contact line of 130 μm. Varying this position has shown to change the absolute contact angle values however the characteristics of the observed hysteresis pattern in Figure 7 are not sensitive to a different choice. However it has been shown in the error analysis, that the receding thickness distribution has a significant error which increasing the distance at which the contact angle is measured. Hence, the distance has been chosen such

GALA e.V., Karlsruhe, Germany, ISBN 978-3-9816764-7-1

that a proper contact angle calculation is possible while keeping the measurement error at the possible minimum.

Conclusion and recommendations for future work

The measurement technique has proven to quantify 3D instantaneous fluid surfaces near moving 3 phase contact lines. These were used to determine contact angle distributions. The results show expected microscopic contact angle values for the advancing and receding contact lines. A stronger contact angle spread was observed for receding contact lines. The experiments have proven that the experimental set-up is capable of measuring microscopic contact angles also for geometrically irregular and instationary 3 phase contact lines. In the future, the algorithm will be extended to take all three laser colours into consideration as this will allow to measure thin films without knowing the exact 0-thickness point and increase the spatial resolution. The theoretical framework to reconstruct a film thickness out of a single point RGB information is set by Kitagawa 2013, which will be used when implementing the code. The technique will be applied to complex wetting situations such as the rise of rivulet in sharp and real-world corners which are modelled for macroscopic contact angles in the work of Gerlach et al. [2020, 2021].

Acknowledgments

The authors would like to thank F. Plückebaum for the technical assistance in the lab and the German Research Association (project number:265191195 – SFB 1194) for funding.

Bibliography

Gerlach, F., Hartmann, M. Hussong, J., Tropea, C., 2021: „Rivulets of finite height“, Colloids and Surfaces A: Physicochemical and Engineering Aspects. 616:126012.

Gerlach, F., Hussong, J., Roisman, I.V, Tropea, C., 2020: “Capillary rivulet rise in real-world corners”. Colloids and Surfaces A. 592:124530.

Kistler, S. F., 1993: “Hydrodynamics of wetting”. Wettability (ed. J. C. Berg). New York: Marcel Decker. pp. 311-429.

Kitagawa, K., 2013: “Thin-film thickness profile measurement by three-wavelength interference colour analysis”. Applied Optics. 52(10):1998-2007.

Pascaline, H., 2016: “Partial Wetting of thin liquid films in polymer tubes”. PhD Thesis. Pierre and Marie Curie University. DOI: 10.13140/RG.2.2.36669.05605

Pinterich, T., Winkler, P.M., Vrtala, A.E., Wagner, P.E., 2011: “Experiments on the contact angle of n-propanol on differently prepared silver substrates at various temperatures and implications for the properties of silver nanoparticles”. Atmospheric Research. 101:510-518.

Takeda, M., Ina, H., Kobayashi, S., 1982: “Fourier-transform method of fringe-pattern analysis for computer-based topography and interferometry”, Journal of the Optical Society of America. 72:156-160.

GALA e.V., Karlsruhe, Germany, ISBN 978-3-9816764-7-1